Electrical Engineering (2025) 107:15005–15023
https://doi.org/10.1007/s00202-025-03309-y

ORIGINAL PAPER

A risk-based framework to enhance post-earthquake resilience in reconfigurable active distribution networks

Mohsen Ghanbarizadeh[1] · Mohsen Simab[2] · Taher Niknam[3]

Received: 28 January 2025 / Accepted: 24 July 2025 / Published online: 11 August 2025

Abstract
Recent seismic events have highlighted the need to enhance the resilience of electrical distribution systems to minimize prolonged service interruptions for end users. This paper introduces a risk-based resilience-oriented framework for reconfiguring active distribution systems to prioritize critical load supply in post-earthquake conditions. The risk-based framework comprises: (1) modeling earthquake characteristics, (2) assessing seismic component failures, and (3) implementing a resilience-focused reconfiguration strategy. Earthquake features are modeled using attenuation relationship, and component failure probabilities are evaluated through fragility curves and Monte Carlo Simulation. A two-step reconfiguration is then employed to restore critical loads using local Distributed Energy Resources (DERs). The first step maximizes the Restored Load Value while ensuring generation adequacy and maintaining a radial network structure. This step is formulated as a Tree Knapsack Problem and solved using a heuristic Depth-First Search-Particle Swarm Optimization approach. The second step validates the security of the reconfigured network using Optimal Power Flow, minimizing voltage deviations as the objective. The proposed methodology is applied to the IEEE 69-bus test system, considering the seismic vulnerabilities of substations, lines, and DERs, as defined by HAZUS. Simulation results demonstrate the framework's effectiveness, showing its potential as a decision-support tool for Distribution System Operators to enhance resilience and ensure critical load supply after earthquakes.

Keywords Active distribution systems · Earthquakes · Resilience enhancement · Reconfiguration

1 Introduction

1.1 Motivation

Modern society relies heavily on electrical infrastructure, which is essential for supporting social, commercial, and industrial activities. However, this infrastructure is increasingly exposed to a range of threats, including natural disasters, cyber-physical threats, and man-made attacks. Traditional power system planning often focuses on credible contingencies, such as *N-1* or *N-2*, but tends to neglect more severe, low-probability, high-impact events, like *N-K* contingencies, which are crucial for ensuring power continuity during extreme scenarios. In addition, the aging of electrical components worsens system vulnerabilities, as many components are widespread and difficult, costly, and time-consuming to replace or retrofit across the entire system [1, 2].

Natural disasters cause substantial damage to electrical infrastructure through distinct mechanisms. Among these, extreme weather events represent the most frequent cause of power disruptions, accounting for approximately 80% of U.S. outages between 2000 and 2023 [3]. While weather-related events primarily affect above-ground infrastructure—such as transmission lines and poles—through

✉ Mohsen Simab
msimab@lar.ac.ir

Mohsen Ghanbarizadeh
mohsen.ghanbarizadeh@iau.ac.ir

Taher Niknam
niknam@sutech.ac.ir

[1] Department of Electrical Engineering, Marv.C., Islamic Azad University, Marvdasht, Iran

[2] Department of Electrical Engineering, University of Larestan, Lar, Iran

[3] Department of Electrical Engineering, Shiraz University of Technology, Shiraz, Iran

predictable mechanisms, earthquakes present fundamentally different challenges. Seismic events can simultaneously damage both above-ground and underground components, including substations, generation plants, distribution lines, and buried cables. Crucially, earthquake damage tends to be more concentrated and structurally severe. Additionally, unlike weather events—where damage patterns are often predictable enough to allow for the pre-positioning of restoration resources—earthquakes strike without warning and typically overwhelm local response capabilities [4]. These differences can result in significant infrastructure damage and high societal costs. For instance, the 2021 Tiburon Peninsula earthquake caused $6.1 billion in economic losses, the 2020 Zagreb earthquake resulted in $8 billion in damages, and the 2021 Fukushima earthquake led to $1.6 billion in losses [5]. In addition to the economic costs, these disasters often result in prolonged power outages. Following Japan's 2011 Tohoku earthquake, 4.6 million customers experienced extended service interruptions [6].

The destructive impact of earthquakes emphasizes the critical need for strategies to reduce their adverse effects on electrical infrastructure. Distribution systems, in particular, are highly vulnerable due to their radial network configurations, insufficient seismic design, and interdependence with other infrastructures. The collapse of nearby buildings or bridges can exacerbate outages and damage the network further. To address these vulnerabilities, a comprehensive approach is necessary to enhance system resilience. This paper proposes a risk-based framework aimed at improving post-earthquake performance by prioritizing the restoration of critical loads, integrating Distributed Energy Resources (DERs), and ensuring operational security under seismic conditions.

1.2 Literature review

The inherently stochastic nature of natural disasters—characterized by unpredictable timing, location, and intensity—poses significant challenges to conventional power system planning. This uncertainty underscores the importance of risk assessment in ensuring grid performance, which typically involves three key components: (1) hazard characterization, (2) vulnerability assessment, and (3) loss identification and mitigation measures. Studies in this field may focus on a single hazard [7–9] or address multiple hazards simultaneously [10]. Additionally, risk assessments may examine electrical infrastructure in isolation or incorporate interdependencies with other critical systems, such as transportation networks and water treatment facilities [11, 12].

Various risk-based approaches have been explored to enhance power system performance against natural disasters. For hurricanes, historical wind speed data and fragility curves have been used in studies such as [7] to estimate annual failure probabilities through fault tree analysis, while digital twin technology has been employed in [8] for real-time component monitoring. Tornado-related research, including [9], has been conducted using graph theory to assess system performance, although flow analysis is often neglected. Scenario-based resilience and cost analyses, as presented in [13, 14], have been applied to compare different pole materials (wood, concrete, steel) under tornado loads. Overhead line vulnerabilities to extreme wind and ice accretion [15, 16], as well as wildfires [17], have also been examined, with dynamic line rating incorporated in [17] to model wildfire impacts on conductor temperature and current flow. Through these diverse methodologies, evolving strategies for improving power system performance across hazards have been demonstrated.

Resilience, as defined by the IEEE Task Force on "Definition and Quantification of Resilience" [18], is the ability of a system to anticipate, absorb, adapt to, and recover from disruptive events while minimizing their magnitude and duration. The multi-phase time-dependent resilience trapezoid introduced in [18] captures the performance of power systems under extreme events, with adaptability to different hazard characteristics. Figure 1 illustrates this concept, where P_0 and P_D represent the system's normal and degraded resilience levels in pre- and post-disturbance states, respectively. The key time intervals include T_e, T_p, T_r, and T are the time of event onset, end of disturbance progression, restoration initiation, and full recovery, respectively. Resilience enhancement measures are classified based on T_e into planning strategies and operational strategies as detailed in Fig. 1.

Seismic planning strategies focus on preemptive measures to enhance system robustness, including substation retrofitting, replacing overhead lines with underground cables in urban areas, anchoring power transformers, optimally allocating DERs, and implementing preventive islanding techniques in power systems. While these measures improve resilience, electrical components respond stochastically to seismic forces, increasing the risk of equipment failure and consumer disruptions following strong earthquakes. Operational strategies, on the other hand, are designed to enhance post-earthquake system recovery. These include mobile power source scheduling, network topology reconfiguration, and switching in distribution systems, all of which help restore functionality and mitigate service disruptions. Table 1 provides a detailed classification of seismic resilience studies in electrical energy systems, comparing the voltage level of the case study, resilience enhancement actions, and vulnerable components considered.

In [10], a multi-risk assessment framework is proposed that supports both operational and planning enhancement measures, considering the impacts of earthquakes and hurricanes. The study identifies substations and transmission lines

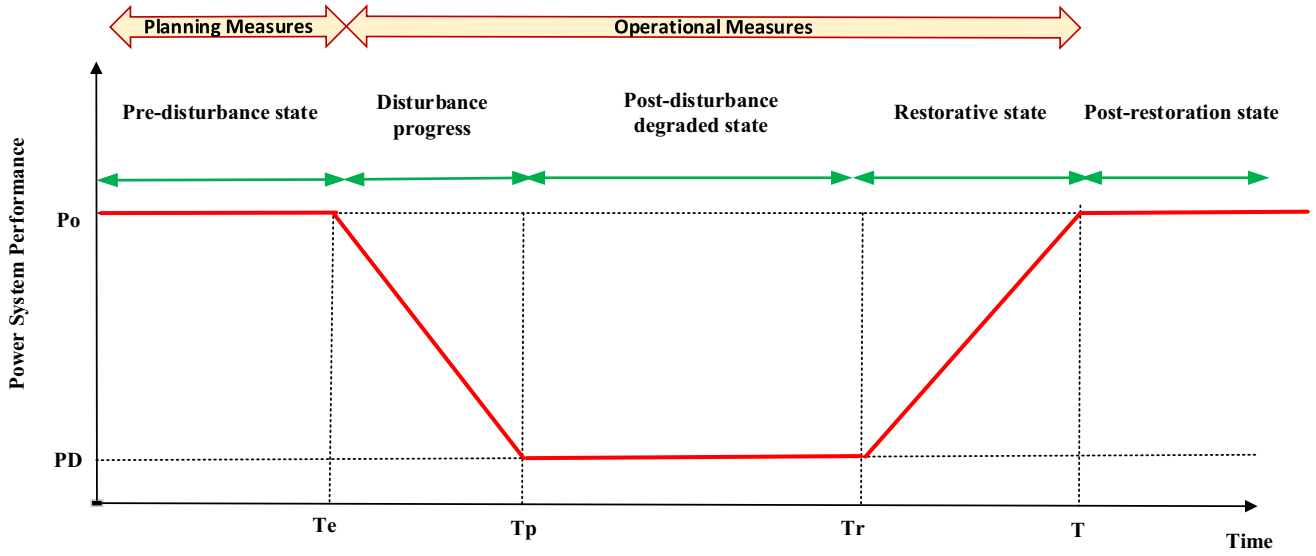

Fig. 1 The multi-phase resilience trapezoid performance curve defined in [18]

Table 1 Literature review of seismic resilience enhancement strategies in power systems—methodologies, system levels, and component vulnerabilities

Reference	Enhancement Measure		Voltage Level		Vulnerable component				
	Planning	Operation	Transmission	Distribution	Substations	Lines		Generation	
						tower	pole	Power Plant	DER
[10]	✓	✓	✓	–	✓	✓	–	–	–
[19]	✓	–	✓	–	✓	–	–	–	–
[20]	✓	–	–	✓	✓	–	✓	–	✓
[21]	✓	–	–	✓	✓	–	–	–	✓
[22]	✓	–	–	✓	✓	–	–	–	✓
[23]	✓	–	✓	–	✓	–	–	✓	–
[24]	✓	–	✓	–	✓	✓	–	✓	–
[25]	✓	–	✓	–	✓	✓	–	✓	–
[26]	–	✓	✓	–	✓	–	–	–	–
[27]	✓	–	–	✓	✓	–	✓	–	–
[28]	✓	–	–	✓	✓	–	✓	–	–
[29]	✓	–	–	✓	✓	–	✓	–	–
[30]	–	✓	–	✓	–	–	✓	–	–
[31]	✓	–	–	✓	–	–	✓	–	–
[32]	–	✓	–	✓	✓	–	✓	–	–
[33]	✓	–	✓	–	–	✓	–	–	–
[34]	✓	–	✓	–	–	✓	–	–	–
[35]	✓	–	✓	–	✓	✓	–	–	–
[36]	✓	–	✓	–	–	✓	–	–	–
[37]	–	✓	✓	–	✓	–	–	–	–
[38]	–	✓	✓	–	✓	–	–	–	–
[39]	–	✓	✓	–	✓	–	–	–	–
This paper	–	✓	–	✓	✓	–	✓	–	✓

as the most vulnerable components for each hazard, respectively. The primary objective is to evaluate system reliability indices. Since substations are among the most vulnerable components of electrical infrastructure during earthquakes, identifying the most at-risk elements within a substation is considered essential for enhancing system resilience. In [19], a statistical analysis was conducted to identify the critical parameters influencing substation vulnerability. The four primary factors found to be most significant are the equipment's year of manufacture, anchoring conditions of heavy equipment, structural integrity of load-bearing elements, and the design of control systems. In several studies [20–22], fault tree analysis has been employed to model substation vulnerabilities as an optimization problem. The objectives in these studies have been set to mitigate Energy Not Supplied (ENS) [20], optimize Risk Reduction Worth (RRW) [21], and minimize the total cost, which includes both interruption and damage expenses [22]. In studies [23–25], the identification of critical substations for retrofitting transmission systems has been prioritized. In [23], Fussell–Vesely (FV) importance measures have been applied to determine critical substations, while DC-Optimal Power Flow (DC-OPF) has been used to estimate ENS. In [24], a two-step Optimization versus Solution (OvS) framework has been introduced, where potential retrofitting solutions are initially selected, followed by the application of DC-OPF to compute ENS. In [25], a decision-dependent probability approach has been proposed for substation retrofitting and expansion planning. The problem has been formulated as a three-level optimization framework, and the Nested Column and Constraint Generation (NC&CG) method has been implemented for its solution. Furthermore, in [26], Bayesian network algorithms have been utilized to develop a probability-based model in which substation functionality is assessed based on the failure probabilities of individual components. This approach allows for a more precise evaluation of substation resilience and supports targeted reinforcement strategies.

In [27, 28], pole retrofitting and Mobile DER allocation are proposed as planning measures. In [27], a stochastic bi-level programming model minimizes investment and interruption costs in the first stage, while reducing load loss in the second stage using a decomposition approach. In [28], a min–max-min model is introduced to minimize planning costs, maximize damage, and reduce load shedding across three stages. In [29], investments in both grid-side and demand-side measures are used to minimize load shedding, modeled as a Mixed-Integer Nonlinear Programming (MINP) problem with a bi-level approach. In [30], a Mixed-Integer Linear Programming (MILP) model is developed for routing mobile DERs to ensure power supply. In [31], batteries are used to maximize supply to critical loads in emergencies, formulated as a Linear Programming (LP) model. Similarly, [32] presents a data-driven LP model for scheduling repairs and allocating mobile DERs.

The interdependence of electrical and gas systems, known as the Integrated Energy System (IES), is explored in [33–35]. In [33], optimal hardening is presented as a multi-level optimization problem, solved using the C&CG method. In [34], a two-stage Distributional Robust Optimization (DRO) problem is proposed to minimize economic losses, with operational costs evaluated using the Weymouth gas flow model and DC-PF. The effects of gas pipeline leaks on utility generation and load curtailment after earthquakes are discussed in [35]. In [36], an attacker-defender model identifies worst-case earthquake scenarios, solved as a two-stage problem using Gurobi. In [37], an equipment repair sequence is proposed to minimize functionality loss, with a Genetic Algorithm (GA) used for optimization. In [38], switching transmission lines is suggested to reduce load curtailment, evaluated with DC-OPF. Finally, [39] aims to minimize generation and curtailment costs during cascading failures, formulated as a MILP model with power flow analysis.

1.3 Gap analysis

While existing studies summarized in Table 1 offer valuable approaches to seismic resilience, they reveal several gaps in the current literature. First, most works focus exclusively on either transmission or distribution systems, neglecting their operational interdependencies. Only a limited number, such as [20], considers both upstream substations and local DERs. Second, prevailing methodologies typically assess component vulnerabilities in isolation, using topology-based proxies such as fault trees or connectivity graphs. This approach overlooks the dynamic, system-wide cascading effects triggered by seismic disruptions, especially those mediated by power flow interdependencies across grid elements. Third, few existing frameworks provide systematic strategies for suppling critical loads after seismic events.

Our proposed framework addresses these gaps through a unified, risk-informed network reconfiguration approach. It integrates probabilistic seismic hazard modeling and component fragility analysis with AC power flow constraints and the operational limits of DERs. In addition, it incorporates a load prioritization mechanism that adapts to post-earthquake system conditions to supply critical loads. This risk-based framework enables adaptive reconfiguration and DER dispatch to maintain the continuity of critical services after seismic events. This capability, as evidenced by the comparative analysis in Table 1.

1.4 Main contributions

This paper employs a standard risk-based reconfiguration framework that accounts for the vulnerabilities of upstream substations, distribution lines, and local DERs, with a focus on integrating probabilistic risk assessment and power flow-based modeling to simulate cascading failures. This approach provides Distribution System Operators (DSOs) with an adaptive strategy to optimize DER utilization, enhance system resilience, and minimize service disruptions after earthquakes. The framework builds on the proven need for active distribution systems to supply critical loads during contingencies [40–44], as demonstrated by the 2011 Japan earthquake and the 2015 Greece wildfire, where local DERs successfully provided backup power [6]. However, previous studies on utilization of DERs to supply critical loads have typically overlooked the specific impacts of natural disasters, such as earthquakes, on distribution systems [45–47]. This paper addresses this significant gap by tailoring the solution to seismic hazards.

The standard risk-based framework begins by incorporating earthquake characteristics, using Peak Ground Acceleration (PGA) as the stress parameter. The second stage evaluates seismic impacts on distribution system components using fragility curves and Monte Carlo Simulation (MCS) to account for the stochastic nature of component failures. In the third stage, a resilience-oriented reconfiguration is proposed, where the distribution system's topological structure is adjusted through the manipulation of switches and tie-switches. This ensures critical loads are supplied through local DERs while adhering to operational constraints through OPF. The main contributions of this paper are summarized below:

- Power Flow-Integrated Probabilistic Risk Assessment for Seismic Resilience: This study uniquely integrates probabilistic seismic risk assessment of distribution system components with network topology modeling and OPF analysis to evaluate cascading failures and identify optimal system reconfigurations under earthquake hazards.
- Modeling and solving the reconfiguration problem: The resilience-oriented reconfiguration is formulated as a two-stage problem to meet the urgent need for fast decision-making in post-earthquake conditions. This approach streamlines the process, enabling quick identification of the optimal reconfiguration to restore power to critical loads and minimize service disruptions,
- Assessment of planning measures effectiveness: The impact of planning measures, such as component retrofitting, on the operational resilience of the distribution system is investigated. Specifically, how these measures influence the performance of the proposed reconfiguration strategy in enhancing the system's ability to recover and maintain service after an earthquake is examined.

It is important to note that although the proposed risk-based resilience-oriented reconfiguration is specifically designed for seismic hazards, it can also be adapted to address other natural disasters or cyber threats by making the necessary adjustments in the first and second stages.

2 Big picture of the proposed framework

2.1 Assumptions

To provide a clear understanding of the framework, the following assumptions are considered: 1. The DSO is responsible for ensuring the supply of critical loads after an earthquake, and load priorities have been predefine;. 2. All DERs within the active distribution network are controllable and can regulate both active and reactive power generation; 3. Controllable switches are installed on all lines, and their status can be adjusted following an earthquakes; 4. The failure probability of overhead lines is assumed to be independent; 5. End-user customers in the distribution system are not vulnerable to post-earthquake conditions, and their demand remains constant; 6. The duration of outages following earthquakes is expected to exceed the capacity of emergency backups, such as batteries, making it necessary to supply critical loads through local DERs. 7. The repair time for the damaged substation is longer than that of the damaged overhead lines. Therefore, the local DERs serve as the only power supply until the substation is restored.

2.2 Risk-based resilience enhancement measures

The proposed framework consists of three stages: (1) incorporating earthquake characteristics using PGA as the stress parameter, (2) assessing seismic impacts on distribution components via fragility curves and MCS, and (3) implementing resilience-oriented reconfiguration by adjusting switches and tie-switches to ensure critical loads are supplied by local DERs while maintaining operational constraints. Figure 2 illustrates the overall structure of the risk-based proposed framework, which will be explained in detail in the following sections.

Stage I: Earthquake modeling

The impacts of natural disasters on electrical components are assessed using specific stress parameters, which are summarized in Table 2.

Seismic faults with high geological risks are identified using historical earthquake catalogs. Geology and seismic engineering principles are then applied to assess potential

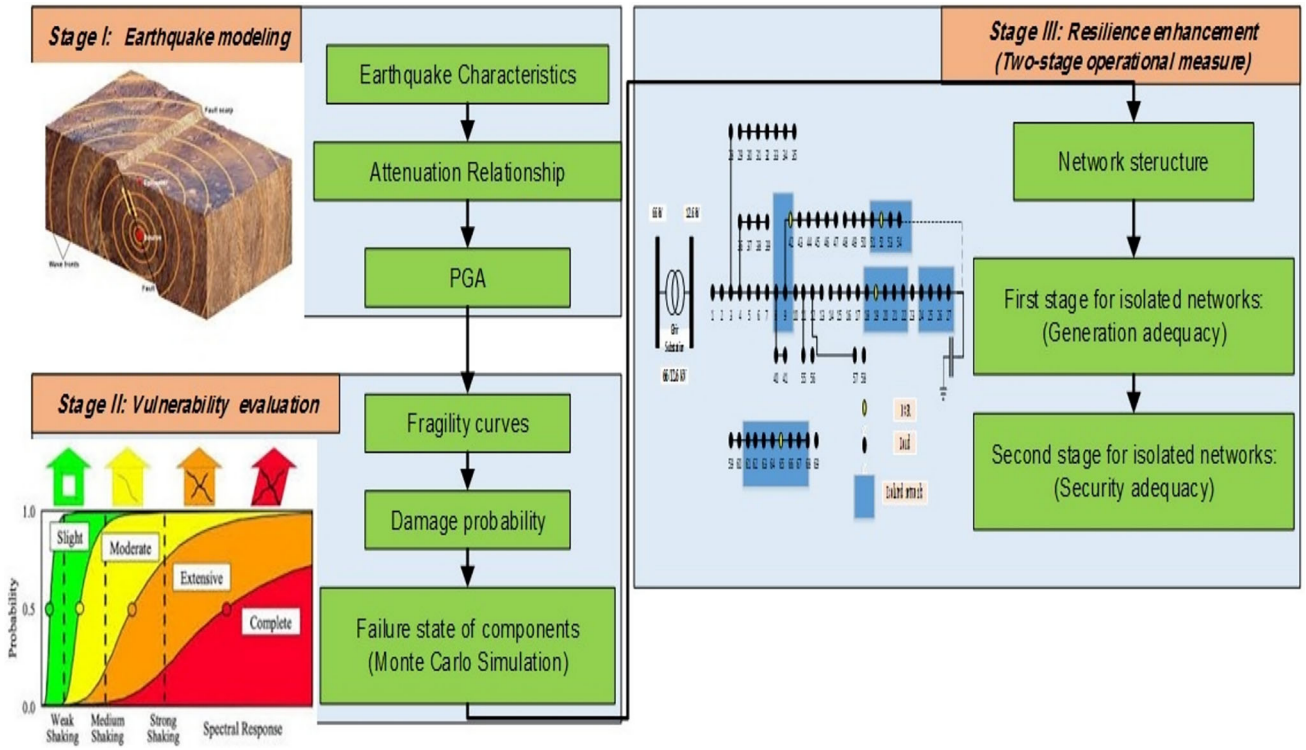

Fig. 2 Big picture of the risk-based resilience enhancement proposed framework against earthquakes

Table 2 Stress parameters are generally considered in risk-based assessment frameworks for natural disasters [48]

Natural disasters	Stress parameters
Lightening	Flash to ground density
Earthquakes	Peak ground acceleration, Peak ground velocity
Wildfires	Temperature and Carbone particle
Ice storms	Wind speed and ice load
Wind storms	Wind Speed
Hurricanes	Wind Speed
Floods	Water level

seismic hazard areas. The propagation and attenuation of seismic energy are significantly influenced by the pattern of earthquake waves, making it crucial to consider the soil type at the locations of electrical components. One key seismic intensity parameter PGA, which measures the maximum horizontal intensity of earthquake shaking experienced by surface-installed components, such as substations, overhead lines, and DERs. PGA plays a vital role in determining the seismic load on electrical infrastructure. To quantify PGA, the general attenuation relationship can be used as follows [49]:

$$\log(PGA) = \psi + F_1(B) + F_2(D) + F_3(\rho) + e \quad (1)$$

The log refers to the natural logarithm. The parameter PGA measured in $\left[\frac{\mathrm{m}}{\mathrm{s}^2}\right]$, which quantifies stress, increases with greater earthquake magnitude (M) in [Mw] and decreases as the distance (D) in [Km] from the epicenter to the component location grows. Factors such as geological site characteristics and the nature of the fault rupture and soil type are incorporated through the function $F_3(\rho)$, where ρ includes these additional variables. A constant term ψ is included in the model, and the uncertainty in PGA is expressed through a random error component, e.

Stage II: Vulnerability of components and evaluation of components failure

Distribution system components, including upstream substations, overhead lines, and DERs, exhibit stochastic behavior under seismic shocks. Their vulnerability is assessed using fragility curves, which estimate the probability of failure based on PGA. Each component's fragility curve follows a lognormal Cumulative Distribution Function (CDF). Fragility curves can be developed using various approaches, including expert judgment, empirical methods, analytical methods, and hybrid techniques. The use of lognormal distributions for fragility curves is a well-established practice in seismic risk assessment, supported by both empirical evidence and theoretical justification [50]. Specifically, the lognormal distribution effectively captures the positive-valued and skewed nature of structural capacity, making it well-suited for modeling seismic performance [51]. The fragility

curve is defined by the logarithmic mean (λ) and standard deviation (β) of the PGA parameter, which represent the thresholds for damage states and their associated variability. The probability that a structure reaches or exceeds a given damage state (ϑ) is expressed by the following [50]:

$$P(\vartheta|S_D) = \Phi \frac{1}{\beta_\vartheta} \ln\left(\frac{S_D}{\lambda_{D,\vartheta}}\right) \tag{2}$$

In this expression, the function Φ denotes the standard Cumulative Distribution Function (CDF) of a lognormal distribution. S_D represents the spectral displacement, while $\lambda_{D,\vartheta}$ indicates its median value. The parameter β_ϑ indicates the standard deviation of the natural logarithm of the spectral displacement at which the structure is likely to enter a specific damage state.

In this paper, the failure probability of a section $P(\text{Failure}|\text{PGA})_{sc}$ is based on Hazus Earthquake Model Technical Manual (chapters 8 and 11). Components are categorized into five damage states: none, minor, moderate, extensive, and complete. To quantitatively assess seismic vulnerability under a given PGA, it is necessary to use fragility curves, which express the probability that a structure will experience a specific damage level or higher. However, estimating the probability of a particular damage state—rather than a cumulative exceedance—requires computing the difference between consecutive fragility curves. Each damage state is further associated with a Damage Ratio (DR), which represents the expected percentage of structural damage as defined in HAZUS. These ratios enable the conversion of probabilistic damage assessments into measurable impacts on infrastructure. The failure probabilities for each damage state and for the component as a whole are provided in Eqs. (3)–(7) and (8), respectively.

$$P_{\text{minor}} = P(\text{minor}|\text{PGA}) - P(\text{moderate}|\text{PGA}) \tag{3}$$

$$P_{\text{moderate}} = P(\text{moderate}|\text{PGA}) - P(\text{extensive}|\text{PGA}) \tag{4}$$

$$P_{\text{extensive}} = P(\text{extensive}|\text{PGA}) - P(\text{complate}|\text{PGA}) \tag{5}$$

$$P_{\text{complate}} = P(\text{complate}|\text{PGA}) \tag{6}$$

$$P_{\text{none}} = 1 - P(\text{minor}|\text{PGA}) \tag{7}$$

$$\begin{aligned} P_{\text{sc}}(\text{Failure}|\text{PGA}) = &\left(P_{\text{minor}} \times \text{DR}_{\text{sc}}^{\text{minore}}\right) \\ &+ \left(P_{\text{moderate}} \times \text{DR}_{\text{sc}}^{\text{moderate}}\right) \\ &+ \left(P_{\text{extensive}} \times \text{DR}_{\text{sc}}^{\text{extensive}}\right) \\ &+ \left(P_{\text{complate}} \times \text{DR}_{\text{sc}}^{\text{complate}}\right) \end{aligned} \tag{8}$$

P_{minor}, P_{moderate}, $P_{\text{extensive}}$, P_{complate}, and P_{none} are the probabilities of failure for the damage states: minor, moderate, extensive, complete, and none, respectively. $\text{DR}_{\text{sc}}^{\text{minore}}$, $\text{DR}_{\text{sc}}^{\text{moderate}}$, $\text{DR}_{\text{sc}}^{\text{extensive}}$, and $\text{DR}_{\text{sc}}^{\text{complete}}$ are the damage ratios for the minor, moderate, extensive, and complete damage states, respectively. Substations' fragility curves are categorized based on voltage levels into high-, medium-, or low-voltage groups. Power generation fragility curves are divided into small and large generation units based on capacity. In this study, upstream grids are modeled as low-voltage substations, while DERs are represented as small power plants. The fragility curve parameters, logarithmic mean value (λ) and logarithmic standard deviation (β), are provided in the corresponding Table 3.

To assess the failure state of components, each iteration of MCS follows a systematic procedure to ensure statistically reliable results. For each component, a random number uniformly distributed between [0,1] is generated. If the component's failure probability exceeds the generated random number, the component is considered to have failed in that iteration; otherwise, it is deemed functional. This process is repeated for all components across multiple MCS iterations. The simulation continues until a predefined stopping criterion is met, ensuring a robust estimation of the system's failure probabilities [52]. Two common stopping rules include halting the simulation when stopping criterion falls below a predefined threshold, and running a fixed number of samples and checking if stopping criterion meets the desired tolerance [53]. MCS exhibits fluctuating convergence, with estimated outputs approaching their true values as the number of simulations increases [53]. To balance accuracy and computational efficiency, a stopping rule is applied based on the coefficient of variation (σ), defined as:

$$\sigma = \frac{\alpha}{E(x)} \tag{9}$$

$E(X)$ is the estimated expectation and α is the standard deviation. A lower σ indicates greater confidence in the results.

The proposed framework allows for evaluating the impact of component retrofitting by simply replacing the fragility curves of non-retrofitted components with those of retrofitted ones. This flexibility enables a seamless assessment of how retrofitting affects overall system performance.

Stage III: Resilience enhancement measure

Quantifying resilience is essential for evaluating and refining enhancement strategies to ensure they remain both actionable and adaptable. In the context of an active distribution system, operational resilience can be assessed using metrics such as the time to recovery of substations (e.g.,$T - T_p$ as illustrated in Fig. 1) and the degradation in system performance (e.g.,$P_0 - P_D$ also shown in Fig. 1). According to

Table 3 Fragility curves of distribution system components for different damage states [50]

Damage Status	Minor		Moderate		Extensive		Complete	
Parameter	λ	β	λ	β	λ	β	λ	β
Non-reinforced Status								
Substation	0.13	0.65	0.26	0.50	0.35	0.40	0.70	0.40
Overhead line	0.24	0.25	0.33	0.20	0.58	0.15	0.89	0.15
DER	0.10	0.50	0.42	0.50	0.42	0.50	0.58	0.50
Reinforced components Status								
Substation	0.15	0.70	0.29	0.55	0.45	0.45	0.90	0.45
Overhead line	0.28	0.30	0.40	0.20	0.72	0.15	0.89	0.15
DER	0.10	0.55	0.21	0.50	0.48	0.50	0.78	0.50

Seismic Resilience Guidelines, utilities are required to pre-identify critical loads and ensure their rapid restoration after disruptive events [54].

In this paper, we propose the Restored Load Value (RLV) as the primary resilience metric, which quantifies the cumulative amount of prioritized critical load restored over time. This metric captures the performance degradation and the speed of recovery, aligning with widely accepted resilience definitions that include robustness, rapidity, and resourcefulness [18]. Critical loads (e.g., hospitals, emergency services) are assigned priority levels based on utility guidelines, and local DERs are deployed via network reconfiguration to supply these loads through isolated networks. This improves P_D and consequently mitigates the total degradation ($P_0 - P_D$), enhancing resilience before full restoration is achieved.

Identifying isolated networks is challenging due to the nonlinear nature of network constraints, which makes direct optimization computationally difficult. To address this, a two-stage approach is used. In the first stage, the problem is simplified by relaxing certain constraints. Specifically, network losses and bus voltage constraints are ignored, transforming the complex MINP problem into a more manageable MILP formulation. This two-stage measure is strategically designed to overcome the computational intractability of solving the full MINLP problem under post-disaster time constraints. The first stage guarantees topological feasibility and critical load prioritization, while the second stage ensures operational viability through power flow analysis, mirroring the actual decision-making hierarchy used by utility operators during emergency response. This allows for efficient preliminary optimization while preserving key structural properties. Critical loads powered by local DERs are selected at the first stage, ensuring that the network maintains a radial structure and meets generation adequacy requirements. In the second stage, an OPF analysis is performed to compute power losses and enforce operational constraints, ensuring feasibility. The objective in this stage is to minimize voltage deviation, which is crucial for maintaining the proper operation of critical loads during emergencies. This two-step framework reduces computational complexity while maintaining solution accuracy, providing a practical and reliable approach to network reconfiguration [55].

3 Problem formulation and solution

3.1 Problem formulation

The key question is how to optimally reconfigure the distribution network to supply critical loads in post-earthquake conditions by DERs while ensuring that security constraints are met. The two-step problem is as follows:

Step One

To address this, the distribution network is modeled as an undirected, node-weighted graph, where each node represents a load, and each edge represents a distribution line. The loads are assigned three different priority levels, represented by weights of 100, 10, and 1 [56]. The highest weight (100) is assigned to critical facilities, such as hospitals, fire stations, food supply centers, and water purification plants. A medium priority (10) is given to gas stations, police stations, and government buildings. Residential customers and other non-critical loads are assigned the lowest priority (1). A criterion called the Restored Load Value (RLV) is introduced in (3) to evaluate the effectiveness of network reconfiguration. By focusing on the RLV, the framework ensures that critical loads are prioritized while maintaining overall system stability and security.

$$\mathrm{RLV}_l = P_l \times W_l \tag{10}$$

RLV_l, P_l, and W_l represent the restored load value, active power, and weight of load l, respectively.

The interrupted loads in post-earthquake condition are the candidates which can be supplied by local DERs. The supplied loads by local DERs must be capable of operating as

isolated networks. In the first stage, power losses and bus voltage constraints are ignored, making it crucial to check generation adequacy and ensure that the radial structure constraints are satisfied. The selection of high-priority loads powered by local DERs is formulated as the (Tree Knapsack Problem) TKP problem. The problem can be expressed as follows:

$$MaxTRLV(\boldsymbol{X}, \boldsymbol{\gamma}) \tag{11}$$

Subject to

$$TRLV(\boldsymbol{X}, \boldsymbol{\gamma}) = \sum_{i \in I} RLV_i(\boldsymbol{X}, \boldsymbol{\gamma}) \tag{12}$$

$$x_c \in \{0, 1\}, \forall c \in \boldsymbol{C} \tag{13}$$

$$\sum_{c \in \boldsymbol{i}} P_c(\boldsymbol{\gamma}) \leq P_{g,i}(\boldsymbol{\gamma}), \forall \, g \in G \tag{14}$$

$$x_c = 1, \forall \, c \in G \tag{15}$$

$$\sum_{(\boldsymbol{a}, \boldsymbol{b}) \in i} \zeta(\boldsymbol{a}, \boldsymbol{b}) = \sum_{c \in i} x_c - 1 \tag{16}$$

$TRLV$ and RLV_i are the total restored load value and the restored load value of island i, respectively. $\boldsymbol{X}$ and $\boldsymbol{\gamma}$ are the set of binary variables and matrix of numbers produced stochastically to determine components failure state, respectively. $\boldsymbol{C}$, $\boldsymbol{I}$, and $\boldsymbol{G}$ are set of candidates, set of isolated networks, and set of DERs, respectively. Moreover, i, c, and g are index of isolated networks, index of candidates, and index of DER nodes, respectively. P_c and $P_{g,i}$ are active power of the candidate c and Generated power of DER_g in island i, respectively. $\zeta(a, b)$ is binary variable demonstrating the edge connection two candidates a and b. If the edge connection is available, $\zeta(a, b) = 1$; otherwise, $\zeta(a, b) = 0$. x_c is the state variable of the candidate selection; if the candidate is selected $x_c = 1$; otherwise, $x_c = 0$.

The objective function is designed to maximize $TRLV$ in post-earthquake conditions. In Eq. (11), the RLV for each isolated network denoted as, RLV_i is calculated. In (13) x_c is the state variable of the candidate selection; if the candidate is selected $x_c = 1$; otherwise, $x_c = 0$. Equation (14) checks the generation adequacy of each isolated network to ensure that it can supply the required power. In Eq. (15), it is assumed that each DER serves as the root of an isolated network and is responsible for supplying other nodes within the isolated network. Finally, Eq. (16) evaluates the radial structure of each island, ensuring that the selected network configuration follows a unique radial structure. This means the number of edges in the network equals the number of selected nodes minus one, by the radial constraint.

Step two

In the second step, power losses and bus voltages are calculated for each isolated network. The objective in this stage is to minimize VD (Voltage Deviation) while ensuring that all operational constraints are met. To achieve this, OPF analysis is applied. The load is divided into two categories: controllable (CL_l) and uncontrollable (UL_l) as follows:

$$P_l = CL_l + UL_l \tag{17}$$

$$CL_l = d_l \times P_l \qquad 0 \leq d_l \leq 1 \tag{18}$$

$$UL_l = e_l \times P_l \qquad 0 \leq e_l \leq 1 \tag{19}$$

P_l, CL_l,and UL_l are active power of the restored load l, uncontrollable part of load l, and controllable part of load l, respectively.

To meet the OPF constraints, the controllable portion of the load is curtailed. Key controller parameters in the OPF process include the curtailment of controllable loads, the reactive power generation from capacitor banks, and the active and reactive power generation from local DERs. The OPF formulation is presented as follows:

$$\text{Min}VD = Min \sum_{c \in i} |U_c - U_{nominal}| \tag{20}$$

Subject to

$$P_i^{\text{loss}} = \sum_{(a,b) \in i} G_{(a,b)} \left(U_a^2 + U_b^2 - 2U_a U_b \cos \emptyset_{ab} \right) \tag{21}$$

$$Q_i^{\text{loss}} = \sum_{(a,b) \in i} B_{ab} \left(U_a^2 + U_b^2 - 2U_a U_b \sin \emptyset_{ab} \right) \tag{22}$$

$$P_c = \sum_{(a,b) \in i} |U_a U_b Y_{ab}| \cos(\theta_a - \theta_b + \emptyset_{ab}) \forall c \in i \tag{23}$$

$$Q_c = \sum_{(a,b) \in i} |U_a U_b Y_{ab}| \sin(\theta_a - \theta_b + \emptyset_{ab}) \forall c \in i \tag{24}$$

$$\sum_{c \in i} P_c + P_i^{\text{loss}} \leq \sum_{g \in i} P_g \tag{25}$$

$$\sum_{c \in i} Q_c + Q_i^{\text{loss}} \leq \sum_{g \in i} Q_g \tag{26}$$

$$U^{\min} \leq U_c \leq U^{\max} \qquad \forall c \in i \tag{27}$$

$$S_{a,b} \leq S_{a,b}^{\max} \quad \forall (a, b) \in i \tag{28}$$

$$P_g^{\min} \leq P_g \leq P_g^{\max} \tag{29}$$

$$Q_g^{\min} \leq Q_g \leq Q_g^{\max} \tag{30}$$

$$0 \leq Q_{\text{cap}} \leq Q_{\text{cap}}^{\max} \tag{31}$$

U_{nominal}, U_c, $U^{\max}$, $U^{\min}$, U_a and U_b are nominal voltage, voltage of node c, maximum voltage, minimum voltage, voltage magnitudes of node a and voltage magnitudes of node b, respectively. Y_{ab}, $G_{a,b}$, and $B_{a,b}$ are admittance magnitude line, real part of the line admittance, and imaginary part of the line admittance connecting nodes (a, b), respectively. P_c and Q_c are active power and reactive power of the candidate c, respectively. $\emptyset_{ab}$, θ_b, and θ_a are phase angel of Y_{ab}, phase of node b, and phase of node a, respectively. $S_{a,b}$ and $S_{a,b}^{\max}$ are the used line capacity and the maximum line capacity connecting nodes a and b, respectively. P_i^{loss} and Q_i^{loss} are active power loss and for isolated network i and reactive power loss and for isolated network i. P_g, $P_g^{\min}$, and $P_g^{\max}$ are active power, minimum active power, and maximum active power generated through DER_g, respectively. Q_g, $Q_g^{\min}$, and $Q_g^{\max}$ are reactive power Minimum reactive power, and Maximum reactive power generation of DER g, respectively. Q_{cap} and $Q_{\text{cap}}^{\max}$ are reactive and maximum reactive power generation of capacitor bank, respectively.

The objective function of the second stage is to minimize voltage deviation in each isolated network as shown in (20). In Eqs. (21) and (22), the active and reactive power losses for the isolated networks are calculated, respectively. Equations (23) and (24) determine the active and reactive powers of the nodes. Equations (25) and (26) evaluate the active and reactive power generation adequacy of the network. Equations (27) and (28) check the voltage and line capacity constraints. In Eqs. (29) and (30), the limitations on active and reactive power generation from DERs are evaluated. Finally, Eq. (31) assesses the reactive power generation limits of the capacitor banks.

3.2 Proposed solution

Step 1: Many nodes may not satisfy the radial and generation adequacy constraints outlined in Eqs. (13–16), and these can be eliminated before solving the optimization problem. The Depth-First Search (DFS) algorithm is applied to identify the nodes that satisfy the constraints (14–16) for each DER. The nodes selected through DFS are then considered candidates for solving the TKP problem presented in Eqs. (12–16). This approach helps to efficiently filter out nodes that cannot meet the necessary constraints before attempting to solve the optimization problem. Algorithm #1 describes the procedure for finding these initial candidates using the DFS method. For more details on the DFS algorithm [57] is referred.

In this paper, Particle Swarm Optimization (PSO) is used to solve the TKP problem. The PSO algorithm is inspired by the cognitive and social behaviors observed in bird flocking. It has been widely applied to various power system challenges, including unit commitment, demand-side management, expansion planning, and reactive power regulation [58]. PSO is easy to understand and implement, requiring only a few parameters, and it achieves stable convergence in a short amount of time [59]. The algorithm defines particles, each representing a potential solution, through a mixture of initial candidates with binary decision variables. Each particle has two attributes: position (S) and velocity (V), both of which are updated in every iteration (it). A particle moves toward the best solution based on its own past experience and the best experience of other particles. The updates for S and V are shown in Eqs. (32) and (33), respectively. The process continues until the best solution is found, determined by evaluating the fitness function.

$$S_s^{it+1} = S_s^{it} + V_s^{it+1} \tag{32}$$

$$V_s^{it+1} = w.V_s^{it} + c_1 r_1^{it}\left(p_s^{it} - S_s^{it}\right) + c_2 r_2^{it}\left(p_g^{it} - S_s^{it}\right) \tag{33}$$

where s is the index of PSO particles, c_1 and c_2 are acceleration constants, r_1 and r_2 are random numbers between [0–1], w and it are inertia weight and counter of iterations, p_g and p_s are the best global point and best individual point for particle s in PSO.

Convert the distribution network structure to an undirected graph structure
Remove the failed lines from the undirected graph structure
Input ,T (Number of DER as the roots of the graph)

1. *for* t=1 : T
2. **Apply** DFS to find the nodes satisfying (14-16) for DER_t
3. **Save** the obtained nodes as candidates to solve problem (12-16)
4. *end for*

Algorithm #2 presents the procedure for solving TKP through PSO, where IT is the number of iterations. More details about PSO can be found in [59].

Input T, (Number of DER as the roots of the graph)
Insert PSO parameters
for t=1 : T
1. **Consider** the obtained nodes from Algorithm #1 for DER_t as the potential solutions
2. **Encode** particles for DER_t
3. **Initialize** P and S for every particle
   for it=1 : IT
4. **Calculate** the fitness function (12-16) for every particle
5. **Update** S and V regarding (32) and (33) for every particle
   end for

The best solution for DER_t is obtained
end for
The best solution for all DERs are obtained

Step 2: DIgSILENT Power Factory has a strong toolbox for distribution systems [60]. In this paper, the OPF is solved with this toolbox.

The summary of the proposed framework and the solution is presented in Fig. 3.

4 Numerical results

4.1 Case study

Iran is located on a major seismic belt and has experienced numerous destructive earthquakes. Ghir, a city in the southern part of Fars Province, near the Ghir fault, was struck by a magnitude 6.5 (Mw) earthquake in 1972 [61]. The seismic data for Ghir used in this study is based on [61, 62], and the attenuation relationship specific to Ghir—presented in Eq. (34)—is based on the characteristics of the central Zagros seismic zone, where the city is located and was developed through a region-specific empirical approach that combines recorded strong-motion data, geological and tectonic features, and regression analysis [49].

$$\log(\mathrm{PGA}) = 5.67 + 0.318\left(\frac{B+0.38}{1.06}\right) - 0.77 Log(D) - 0.016D \quad (34)$$

To assess the impact, the city is divided into three seismic zones based on the distance from the earthquake's epicenter to various components, and three different PGAs are calculated. The parameters for the fragility curves are provided in Table 3. It is important to note that all components are in a non-reinforced state.

The city is supplied by a 66/12.6 kV substation. It is assumed that one feeder of the distribution system is similar to the IEEE-69 bus system, with the single-line diagram shown in Fig. 4. The total active power demand is 3,802.19 kW, while the reactive power demand is 2694.60 kVAr [63]. The maximum line capacity is 150 A, and the voltage rating is 12.6 kV. The voltage limits are set to 0.95 per-unit for the minimum voltage ($U^{\min}$) and 1.05 per-unit for the maximum voltage ($U^{\max}$). The installed DERs provide 820 kW. Small gas turbines have been installed within the system to support critical loads in post-earthquake conditions, as detailed in Table 4. The power factor of the DERs can be adjusted within the range of [0.8 lead, 0.8 lag]. Additionally, a set of capacitor banks with a total capacity of 600 kVar is installed at node 27 to support voltage regulation and reactive power compensation. A detail of the load priority is presented in Table 5. The customers are divided into controllable, partly controllable, and uncontrollable sections, as shown in Table 6. PSO parameters are shown in Table 7, where N_p is the population size.

4.2 Basic scenario

In the base scenario which is a snapshot of earthquake damages, the earthquake epicenter is located 15 km, 20 km, and 25 km from the equipment in zones 1, 2, and 3, respectively. The earthquake has a magnitude of 6.5 Mw. Using the attenuation relation in Eq. (34), PGAs are calculated for each seismic zone, followed by MCS to assess component failures. The resulting PGAs and failed components are summarized in Table 8. The upstream substation and eight distribution lines fail due to the earthquake. The substation failure disconnects the entire distribution system from the upstream grid. To restore power, the proposed method is applied, identifying

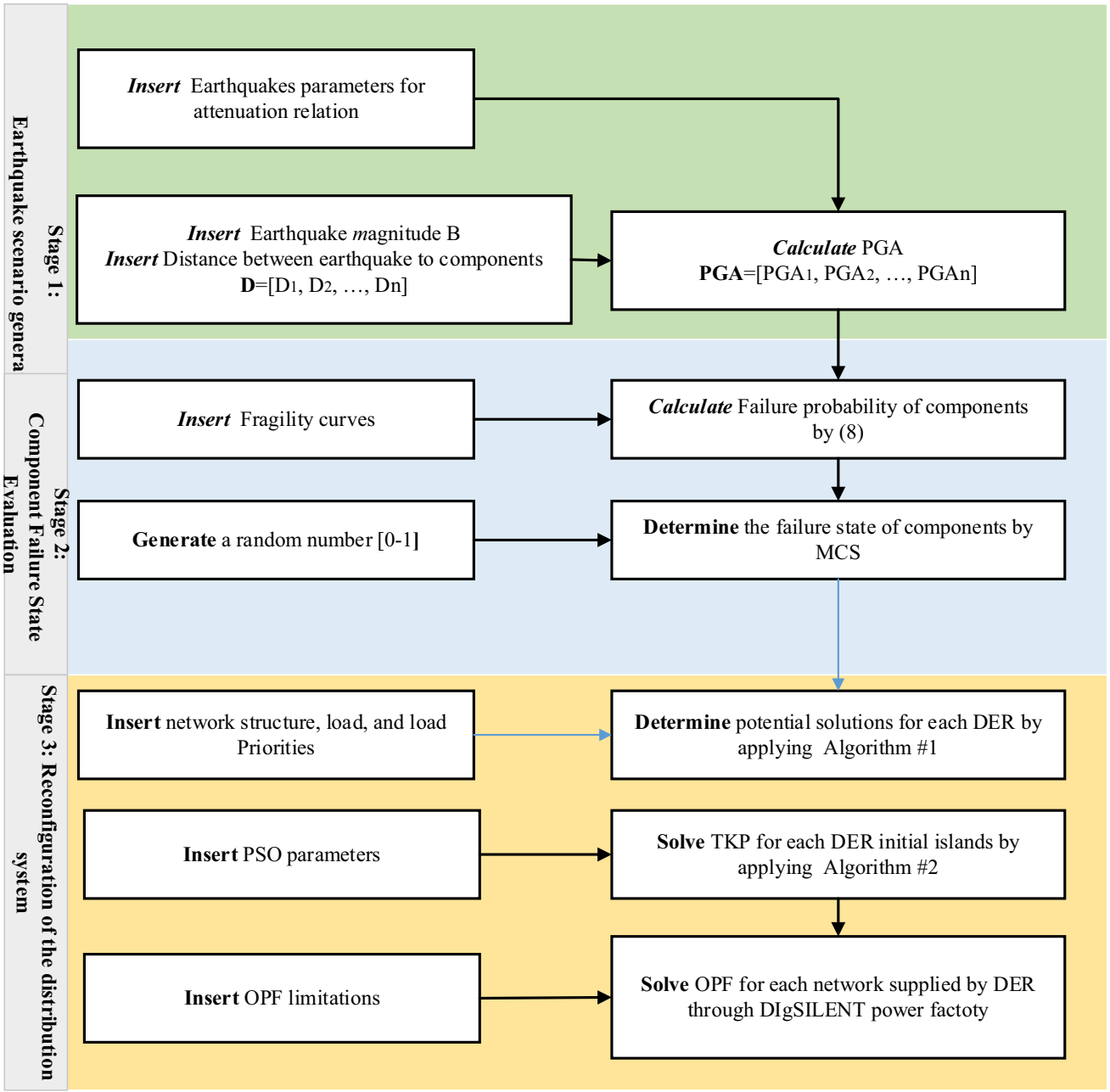

Fig. 3 The three-stage risk-based resilience-oriented framework against earthquakes

feasible isolated networks, as shown in Fig. 5 and Table 9. Through Depth-First Search (DFS), DER1 and nodes 14–27 are selected as potential candidates. PSO is then applied, selecting nodes 18–22 to be supplied by DER1.

In the second stage, OPF is executed, resulting in a power loss of 1.2 kW within the selected island. A similar restoration process is applied for other DERs. The total RLV is 29,750 units, the total restored loads is 763.05 kW, the total power loss and reactive loss are 5.2 kW and 2.02 kVar, respectively. Additionally, the capacitor bank generates 600 kVAR of reactive power, and the DER power factor is set to 0.95 (lead) for all units. To satisfy OPF constraints, the controllable portion of the load at node 24 is curtailed.

4.3 Scenario analysis of earthquake magnitude

In this section, the earthquake magnitude varies, while the distance to components remains constant. Table 10 presents the calculated PGAs for different seismic zones. For consistency, all loads are assigned equal weights (weight = 1), meaning the restored load is equal to the *RLV*. Given the stochastic nature of the seismic response, MCS is performed

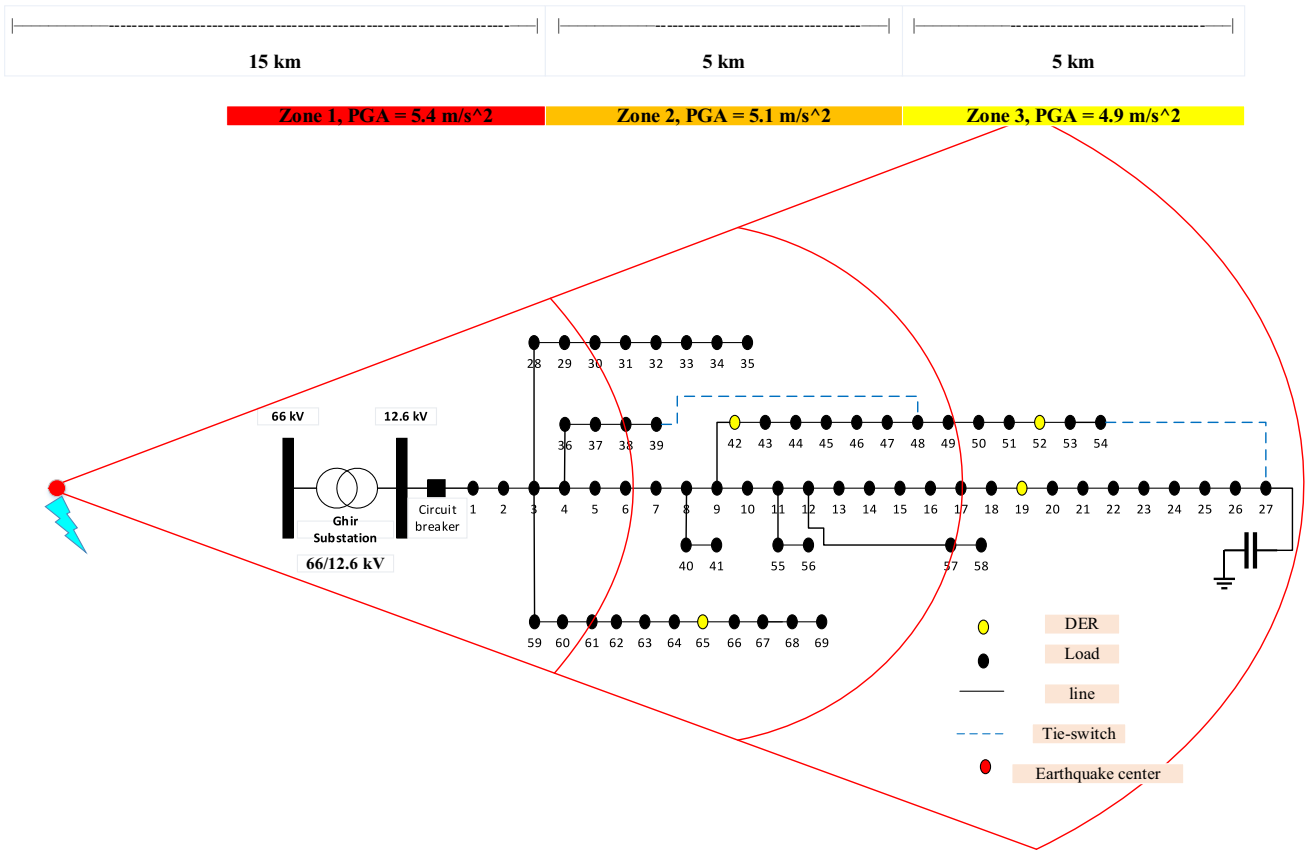

Fig. 4 Single line diagram of IEEE-69 bus system divided into three seismic zones

Table 4 Characteristics of 4 DERs installed to IEEE 69-bus system

DER Number	1	2	3	4
Node number	19	42	52	65
Capacity (kW)	200	120	400	100

Table 5 Details of the three types of priority of loads

Priority type	Weight	Node number
High	100	6, 9, 12, 18, 35, 37, 42, 51, 57, 62
Medium	10	Other nodes
Low	1	7, 10, 11, 13, 16, 22, 28, 38, 43–48, 60, 63

Table 6 Characteristics of customer's load shedding

Node number	Load type	*e*	*d*
Other nodes	Uncontrollable	1	0
26, 27, 34, 39,41, 43–44, 48, 53–56,58, 66–69	Controllable	0	1
11, 13,16, 21, 38, 24	Partly controllable	0.4	0.6

until the stopping criterion—$\alpha \leq 0.05$—is satisfied, ensuring statistically reliable results across various possible isolated network configurations [53]. The proposed reconfiguration method is then applied, and the results are illustrated in Fig. 6. The findings reveal that for weak earthquakes, the restored load is minimal as the damage to the distribution system is negligible. As the earthquake intensity increases, the restored load grows, primarily due to substation failure, which forces DERs into islanded operation and makes reconfiguration more effective. However, for strong earthquakes (magnitude 7 +), the restored load drops sharply due to the high vulnerability of DERs, limiting their ability to maintain power supply. The restored loads for different earthquake magnitudes are 112 kW, 350 kW, 472 kW, 765 kW, 632 kW, and 231 kW, with the restored load decreasing by 18% from magnitude 6 to 7 and 70% from magnitude 6 to 8. This demonstrates that DER-based reconfiguration is effective for earthquakes but becomes increasingly ineffective as earthquake intensity rises dramatically, highlighting the importance of earthquake-resilient DERs, such as photovoltaic power plants, in regions prone to high-magnitude earthquakes.

Table 7 PSO parameters applied for simulation

Parameter	Np	w	c_1	c_2	IT
Quantity	200	1.2	1.2	0.9	2000

Table 8 Seismic data and components failure data regarding the basic scenario

Seismic zone	Distance (km)	PGA $\left(\frac{m}{s^2}\right)$	Failed components
Zone 1	15	5.4	Substation, Line (3,59), Line (68,69), Line (28,29)
Zone 2	20	5.1	Line (55, 56), Line (39, 48), Line (47, 48),
Zone 3	25	4.9	Line (13, 14), Line (57–58)

4.4 Evaluation the effect of components retrofitting

This section evaluates the effect of component retrofitting on the proposed resilience framework. To achieve this, the fragility curve parameters for retrofitted components, as shown in Table 3, replace those used in the previous simulations, while all other assumptions remain unchanged. The results, compared to the non-retrofitted scenario, are illustrated in Fig. 7. The findings indicate that retrofitting components before an earthquake, combined with post-event network reconfiguration, significantly enhances resilience. Strengthening the upstream substation helps prevent distribution system disconnection from the main grid, reducing the need for reconfiguration. However, for high-magnitude earthquakes where substation failure is inevitable, the ability of local DERs to supply critical loads becomes crucial for maintaining system operation.

In the non-retrofitted scenario, the interrupted loads increase significantly with earthquake intensity, reaching 200 kW, 1001 kW, 1410 kW, 2009 kW, 3154 kW, and 3602 kW for magnitudes 3, 4, 5, 6, 7, and 8, respectively. When retrofitting measures are applied, these values drop to 49 kW, 204 kW, 506 kW, 609 kW, 812 kW, and 1222 kW, highlighting a significant improvement. However, in extreme earthquakes (magnitude 8), power interruptions remain substantial (1222 kW) due to the simultaneous failure of both the substation and local DERs. This emphasizes the limitations of retrofitting alone and the need for a comprehensive resilience strategy, incorporating DER reinforcement, alternative power sources to further mitigate disruptions during severe seismic events.

4.5 Comparison with other methods

To assess the efficiency of the proposed resilience enhancement method, its results are compared with the approaches presented in [64]. In [64], isolated networks are only permitted when the total DER generation exceeds the total load in the isolated network. If the total load surpasses the DER capacity, the isolated network is not allowed, leading to a failure in the resilience enhancement process, and the DERs must be shut down. For instance, in the network snapshot from Section IV-B, the total load in every isolated network exceeds DER generation under [64], preventing any load restoration and resulting in a *RLV* of zero.

In contrast, the proposed method offers superior resilience performance by ensuring that critical loads can still be supplied, even when the upstream grid is disconnected or when the total interrupted load is less than the available DER generation. To comprehensively evaluate system performance under different damage scenarios, the basic scenario from Section IV-B was repeated, with results summarized in Table 11. The findings demonstrate that the average *VRL* obtained using the proposed method is significantly higher than that of [64]. This improvement highlights the key advantage of the proposed approach—its ability to dynamically reconfigure the network, optimally allocate DER resources, and maintain power supply to critical loads under extreme conditions, making it a more effective and reliable resilience strategy.

4.6 Scenario analysis of DER penetration

This section investigates the effects of DER penetration on the distribution system's performance through scenario-based analysis. The study assumes that DERs are directly connected to the 12.6 kV distribution network, with their cumulative capacity limited to 60% of the feeder's total load (2,281.2 kW). The DER portfolio consists of four units (DER1–DER4), contributing 12.2%, 48.8%, 14.6%, and 24.4% of the total DER capacity, respectively. The seismic scenario and input data align with the baseline conditions defined in Section IV.B.

MCS were conducted for varying DER penetration levels, with the results summarized in Table 12. The analysis reveals that higher DER penetration increases *RLV*. However, the rate of *RLV* growth diminishes at elevated penetration levels. This nonlinear trend is attributed to the vulnerability of distribution lines, which constrains the system's ability to fully utilize available DER generation for supplying additional loads.

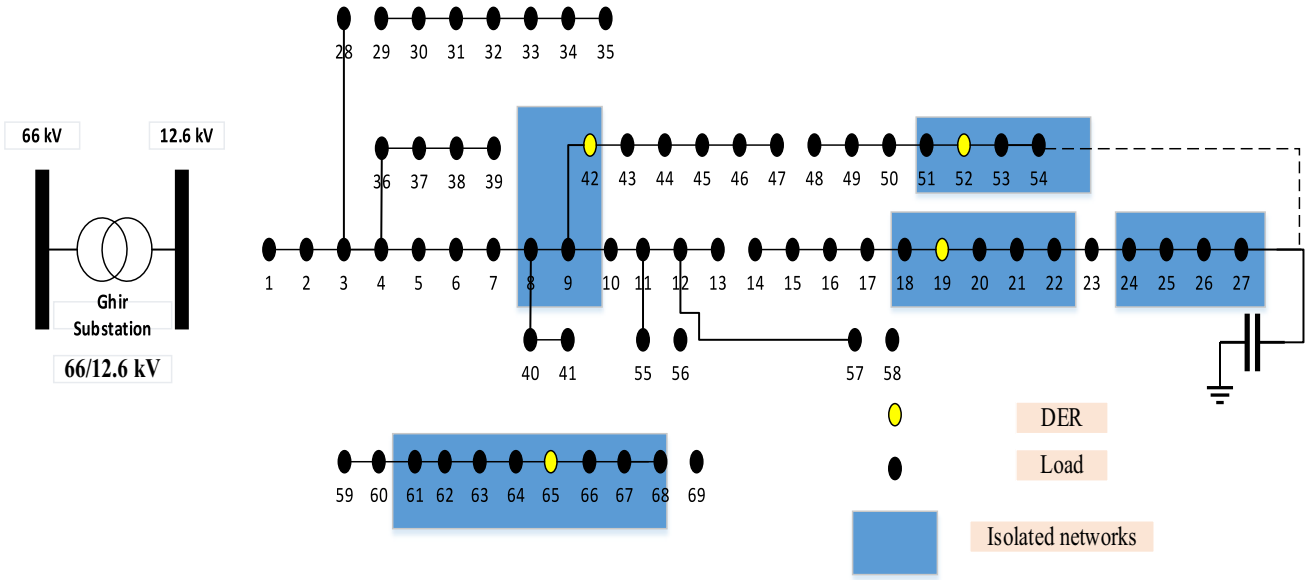

Fig. 5 Isolated networks supplied by local DERs regarding the basic scenario

Table 9 Details of the isolated networks supplied by local DERs regarding the basic scenario

DER Number	First stage			RLV	Second Stage		
	PSO particles	Selected nodes	Restored loads (kW)		Active Power loss (kW)	Reactive Power loss (kVar)	VD (p.u)
1	14–27	18–22	180.3	7155	1.2	0.56	0.01
2	8–10, 43–47	8,9,42	109.35	4185	1.1	0.42	0.02
3	18–27, 51–54	24–27, 51–54	379	13,780	2	0.67	0.01
4	59–69	61–68	94.4	4630	0.9	0.37	0.01
Total			763.05	29,750	5.2	2.02	

Table 10 The calculated PGA for scenario analysis of earthquake magnitude

Seismic zone	Magnitude (Mw)					
	3	4	5	6	7	8
PGA Zone 1	0.44	0.47	0.50	0.53	0.56	0.59
PGA Zone 2 $\left(\frac{m}{s^2}\right)$	0.41	0.44	0.47	0.50	0.52	0.56
PGA Zone 3 $\left(\frac{m}{s^2}\right)$	0.38	0.41	0.44	0.47	0.50	0.53

5 Conclusion and future works

5.1 Conclusion

This paper introduces a risk-based reconfiguration framework for active distribution systems in seismic hazard conditions. The framework consists of earthquake modeling, vulnerability assessment, and resilience-oriented reconfiguration, formulated as a two-step optimization problem. The effectiveness and flexibility of the proposed method were demonstrated through extensive simulations. In Section IV-C, the impact of earthquake intensity on distribution system

Table 11 Comparison of the proposed method with the methods proposed in [64]

	Method in this paper	Method in [64]
Restored loads (kW)	772	245
RLV	29,654	9,320

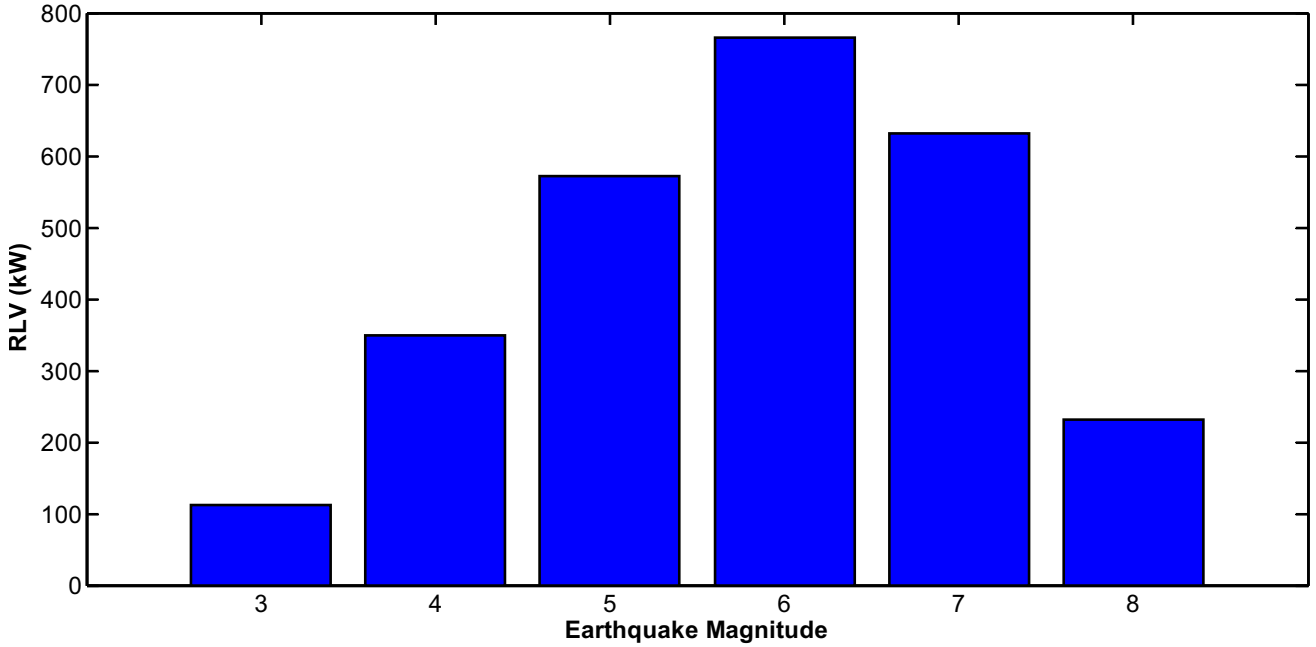

Fig. 6 Restored load through the proposed reconfiguration approach for different earthquake magnitude

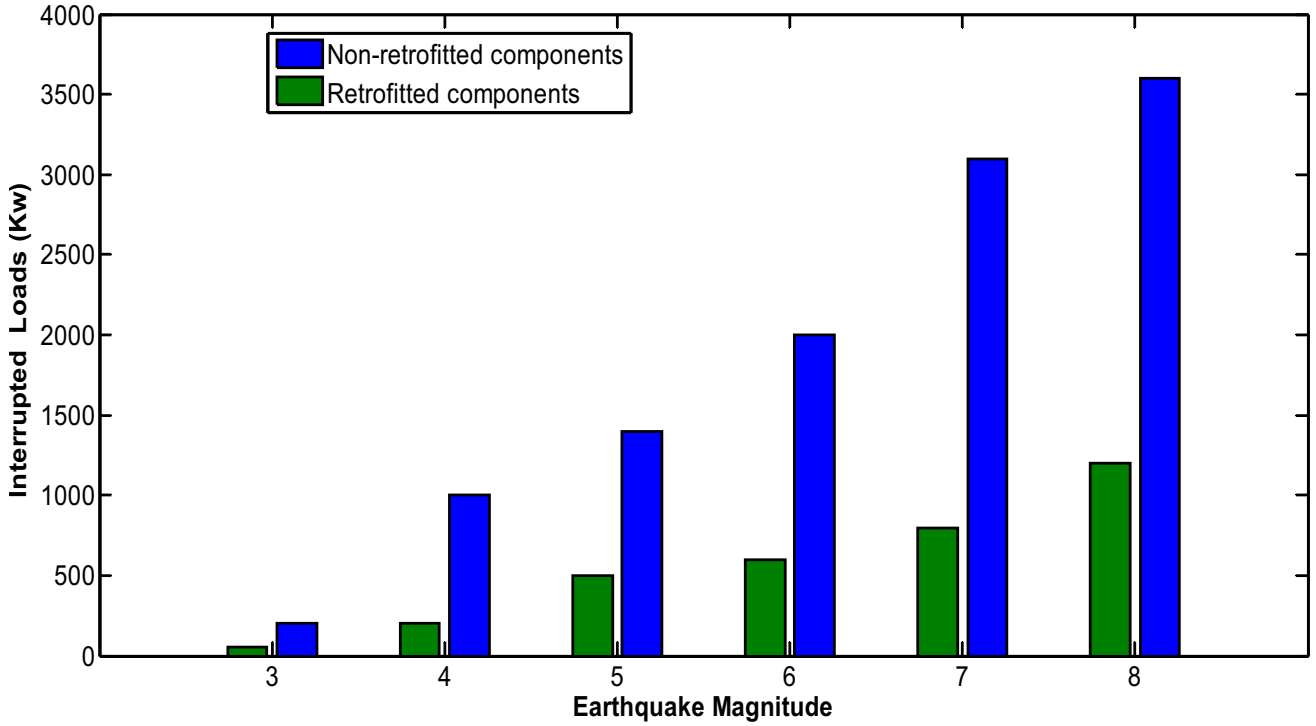

Fig. 7 Comparison of the power interruption for retrofitted and non-retrofitted components

Table 12 Results of scenario analysis of DER penetration for the basic case study

DER penetration (%)	0	10	20	30	40	50	60
Generation Capacity (Kw)	0	380.2	760.4	1140.6	1520.8	1901	2281.2
RLV	0	13,537	24,752	44,521	55,675	65,231	68,778

performance was analyzed, revealing that DER-based islanding becomes essential when substation failures occur. In Section IV-D, the benefits of component retrofitting were evaluated, showing that reinforcing critical infrastructure significantly enhances resilience. Additionally, in Section IV-E, an alternative reconfiguration strategy was examined, further demonstrating the proposed method's superiority in maintaining power supply to critical loads. The results highlight that combining planning measures (component retrofitting) with operational measures (reconfiguration) significantly improves system resilience. In Section IV-F, the benefits of high DER penetration for resilience enhancement is demonstrated. By leveraging local DERs and adaptive reconfiguration, this framework provides a more effective and practical solution for post-disaster power restoration. Ultimately, the proposed method serves as a valuable decision-support tool for distribution system operators (DSOs), enabling faster and more reliable recovery in earthquake-affected regions.

5.2 Limitations and future works

This study focused on controllable DERs, such as gas turbines and diesel generators, which can regulate active and reactive power generation after earthquakes, with their failure being the only uncertainty considered. Future research will explore the advantages and challenges of renewable energy sources like wind turbines and photovoltaic systems, which introduce greater uncertainty in power generation but may enhance resilience in supplying critical loads. Additionally, this study assumed that end-user buildings and infrastructure remain undamaged during earthquakes. Investigating building vulnerability would provide valuable insights into end-user disruptions and could account for overhead line failures caused by collapsing structures. Another limitation is the neglect of underground cable damage due to seismic activity. Future studies should identify key stress parameters such as Peak Ground Velocity (PGV) and Peak Ground Displacement (PGD) for underground cables and compare the resilience of overhead lines and underground cable systems in seismic conditions [65]. One key limitation of this study is the use of generalized fragility curves, which do not capture the effects of aging infrastructure or substation-specific layout due to limited publicly available data. As a result, the accuracy of loss estimates may be affected by these unmolded real-world complexities. Future work should incorporate more advanced, region-specific vulnerability models beyond HAZUS to enhance the realism and precision of the simulations. On the other hand, assessing substation layouts (e.g., single bus-bar, double bus-bar, etc.) and evaluating the impact of design standards—such as IEEE 693, which specifies the ability to withstand a Peak Ground Acceleration (PGA) of 0.5 g without failure—can be considered practical measures for enhancing planning and resilience. Addressing these aspects will help refine disaster-response strategies and improve the overall resilience of distribution networks.

Author contributions All authors contributed to the study conception and simulation. Mohsen Ghanbarizadeh took part in methodology, software, validation, formal analysis, investigation, resources, data curation,writing. Mohsen Simab involved in conceptualization, methodology, software, validation, formal analysis. Taher Niknam took part in methodology, resources, data curation, writing—original draft, Supervision, project administration.

Data availability No datasets were generated or analysed during the current study.

Declarations

Competing Interests The authors declare no competing interests.

References

1. Oboudi MH, Hamidpour H, Zadehbagheri M, Safaee S, Pirouzi S (2024) Reliability-constrained transmission expansion planning based on simultaneous forecasting method of loads and renewable generations. Electr Eng. https://doi.org/10.1007/s00202-024-02556-9
2. Pirouzi S, Zadehbagheri M, Behzadpoor S (2024) Optimal placement of distributed generation and distributed automation in the distribution grid based on operation, reliability, and economic objective of distribution system operator. Electr Eng. https://doi.org/10.1007/s00202-024-02458-w
3. Rahim MA (2024) Unveiling weather-induced blackouts: a ten-year analysis with deep learning-driven power resilience enhancement. IEEE Access 12:1–15
4. Wang Y, Chen C, Wang J, Baldick R (2015) Research on resilience of power systems under natural disasters—a review. IEEE Trans Power Syst 31(2):1604–1613
5. Mohsen RA, Shivaie M (2022) A seismic-resilient multi-level framework for distribution network reinforcement planning considering renewable-based multi-microgrids. Appl Energy 325(1):119824. https://doi.org/10.1016/j.apenergy.2022.119824
6. Marnay C, Aki H, Hirose K, Kwasinski A, Ogura S, Shinji T (2015) Japan's pivot to resilience: how two microgrids fared after the 2011 earthquake. IEEE Power Energy Mag 13(3):44–57. https://doi.org/10.1109/MPE.2015.2397333
7. Salman AM, Li Y, Stewart MG (2015) Evaluating system reliability and targeted hardening strategies of power distribution systems subjected to hurricanes. Reliab Eng Syst Saf 144:319–333
8. Braik AM, Koliou M (2023) A novel digital twin framework of electric power infrastructure systems subjected to hurricanes. Int J Disaster Risk Reduct 97:Art. no. 104020
9. Unnikrishnan VU, van de Lindt JW (2016) Probabilistic framework for performance assessment of electrical power networks to tornadoes. Sustain Resilient Infrastruct 1(3–4):137–152
10. Salman AM, Li Y (2017) Multihazard risk assessment of electric power systems. J Struct Eng 143(3):04016198
11. Perelman G, Shmaya T, Navon A, Vrachimis S, Panteli M, Eliades DG, Ostfeld A (2025) Coordinated operational optimization of water and power systems under emergency conditions. Sustain Energy Grids Netw 2025:101643
12. Braik AM, Koliou M (2024) A digital twin framework for efficient electric power restoration and resilient recovery in the aftermath

of hurricanes considering the interdependencies with road network and essential facilities. Resilient Cities Struct 3(3):79–91
13. Braik AM, Salman AM, Li Y (2019) Risk-based reliability and cost analysis of utility poles subjected to tornado hazard. J Aerosp Eng 32(4):04019040
14. Braik AM, Salman AM, Li Y (2020) Reliability-based assessment and cost analysis of power distribution systems at risk of tornado hazard. ASCE-ASME J Risk Uncertain Eng Syst Part A Civ Eng 6(2):04020014
15. Ma Y, Dai Q, Pang W (2020) Reliability assessment of electrical grids subjected to wind hazards and ice accretion with concurrent wind. J Struct Eng 146(7):04020134
16. Hou G et al (2023) Resilience assessment and enhancement evaluation of power distribution systems subjected to ice storms. Reliab Eng Syst Saf 230:108964
17. Trakas DN, Hatziargyriou ND (2017) Optimal distribution system operation for enhancing resilience against wildfires. IEEE Trans Power Syst 33(2):2260–2271
18. IEEE Task Force (2018) The definition and quantification of resilience. Accessed: 2018–08- 03. [Online]. Available:http://resourcecenter.ieee-pes.org/pes/product/technicalpublications/PESTR006504-18
19. Jaigirdar MA (2005) Seismic fragility and risk analysis of electric power substations. M.S. thesis, Dept. Civ. Eng., Univ. of Buffalo, Buffalo, NY, USA
20. Oboudi MH, Mohammadi M (2024) Two-stage seismic resilience enhancement of electrical distribution systems. Reliab Eng Syst Saf 241:109635. https://doi.org/10.1016/j.ress.2023.109635
21. Oboudi MH, Mohammadi M, Trakas DN, Hatziargyriou ND (2023) A risk-based framework to improve a distribution system's resilience against earthquakes. J Energy Eng 149(1):04022049. https://doi.org/10.1061/JLEED9.EYENG-4586
22. Oboudi MH, Mohammadi M, Trakas DN, Hatziargyriou ND (2021) A systematic method for power system hardening to increase resilience against earthquakes. IEEE Syst J 15(4):4970–4979. https://doi.org/10.1109/JSYST.2020.3032783
23. Espinoza S, Poulos A, Rudnick H, de la Llera JC, Panteli M, Mancarella P (2020) Risk and resilience assessment with component criticality ranking of electric power systems subject to earthquakes. IEEE Syst J 14(2):2837–2848. https://doi.org/10.1109/JSYST.2019.2961356
24. Lagos T, Moreno R, Espinosa AN, Panteli M, Sacaan R, Ordonez F, Rudnick H, Mancarella P (2020) Identifying optimal portfolios of resilient network investments against natural hazards, with applications to earthquakes. IEEE Trans Power Syst 35(2):1411–1421. https://doi.org/10.1109/TPWRS.2019.2945316
25. Alvarado D, Moreno R, Street A, Panteli M, Mancarella P, Strbac G (2022) Co-optimizing substation hardening and transmission expansion against earthquakes: a decision-dependent probability approach. IEEE Trans Power Syst 38(3):2058–2070. https://doi.org/10.1109/TPWRS.2022.3180363
26. Liu X, Xie Q (2024) A multi-strategy framework to evaluate seismic resilience improvement of substations. Reliab Eng Syst Saf 245(1):110045. https://doi.org/10.1016/j.ress.2024.110045
27. Shi W, Liang H, Bittner M (2023) Stochastic planning for power distribution system resilience enhancement against earthquakes considering mobile energy resources. IEEE Trans Sustain Energy. https://doi.org/10.1109/TSTE.2023.3296063
28. Ahmadi M, Bahrami M, Vakilian M, Lehtonen M (2020) Application of hardening strategies and dg placement to improve distribution network resilience against earthquakes. IEEE PES Transmission & Distribution Conference and Exhibition-Latin America (T&D LA), pp 1–6
29. Saini DK, Sharma M (2021) Techno-economic hardening strategies to enhance distribution system resilience against earthquake. Reliab Eng Syst Saf 213(1):107682. https://doi.org/10.1016/j.ress.2021.107682
30. Yang Z, Dehghanian P, Nazemi M (2020) Seismic-resilient electric power distribution systems: harnessing the mobility of power sources. IEEE Trans Ind Appl 56(3):2304–2313. https://doi.org/10.1109/TIA.2020.2972854
31. Nazemi M, Moeini-Aghtaie M, Fotuhi-Firuzabad M, Dehghanian P (2020) Energy storage planning for enhanced resilience of power distribution networks against earthquakes. IEEE Trans Sustain Energy 11(2):795–806. https://doi.org/10.1109/TSTE.2019.2907613
32. Shi W, Liang H, Bittner M (2024) Data-driven resilience enhancement for power distribution systems against multishocks of earthquakes. IEEE Trans Ind Inf. https://doi.org/10.1109/TII.2024.3359437
33. Hasanzad F, Rastegar H (2022) Application of optimal hardening for improving resilience of integrated power and natural gas system in case of earthquake. Reliab Eng Syst Saf 223(1):108476. https://doi.org/10.1016/j.ress.2022.108476
34. Zhao PCGu, Cao Z, Shen Y, Teng F, Chen X, Wu C, Huo D, Xu X, Li S (2021) Data-driven multi-energy investment and management under earthquakes. IEEE Trans Ind Informat 17(10):6939–6950. https://doi.org/10.1109/TII.2020.3043086
35. Shen Y, Gu C, Yang X, Zhao P (2021) Impact analysis of seismic events on integrated electricity and natural gas systems. IEEE Trans Power Deliv. https://doi.org/10.1109/TPWRD.2020.3017050
36. Oneto A, Lorca Á, Ferrario E, Poulos A, Carlos De La Llera J, Negrete-Pincetic M (2024) Data-driven optimization for seismic-resilient power network planning. Comput Oper Res 166(1):10662. https://doi.org/10.1016/j.cor.2024.106628
37. Liang H, Xie Q (2023) Resilience-based sequential recovery planning for substations subjected to earthquakes. IEEE Trans Power Deliv. https://doi.org/10.1109/TPWRD.2022.3187162
38. Nazemi M, Dehghanian P (2020) Seismic-resilient bulk power grids: hazard characterization, modeling, and mitigation. IEEE Trans Eng Manage 67(3):614–630. https://doi.org/10.1109/TEM.2019.2950669
39. Cheng B, Nozick L, Dobson I (2022) Investment planning for earthquake-resilient electric power systems considering cascading outages. Earthq Spectra. https://doi.org/10.1177/8755293022 1076870
40. Islam MT, Hazra J, Singh AK (2023) Resilience enhancement methods for electric power distribution systems: a review. Renew Sustain Energy Rev 181:113321. https://doi.org/10.1016/j.rser.2023.113321
41. Liu W, Wang B, Dong X (2020) Distributed generation and microgrids for enhancing the resilience of electrical distribution systems: a review. IET Energy Syst Integr 2(3):223–231. https://doi.org/10.1049/iet-esi.2019.0134
42. Aziz T, Waseem M, Liu S, Lin Z (2022) Two-stage MILP model for optimal skeleton-network reconfiguration of power system for grid-resilience enhancement. J Energy Eng. https://doi.org/10.1061/(ASCE)EY.1943-7897.0000814
43. Pang K, Wang C, Wen F, Palu I, Feng C, Yang Z, Chen M, Zhao H, Shang H (2020) Two-stage self-healing restoration strategy considering operating performance. J Energy Eng. https://doi.org/10.1061/(ASCE)EY.1943-7897.0000683
44. IEEE (2011) IEEE guide for design operation and integration of distributed resource island systems with electric power systems. IEEE 1547.4. New York: IEEE
45. Oboudi MH, Mohammadi M, Rastegar M (2019) Resilience-oriented intentional islanding of reconfigurable distribution power systems. J Mod Power Syst Clean Energy 7(4):741–752. https://doi.org/10.1007/s40565-019-0567-9

46. Xu J, Xie B, Liao S, Yuan Z, Ke D, Sun Y, Peng X (2021) Load shedding and restoration for intentional island with renewable distributed generation. J Mod Power Syst Clean Energy 9(3):612–624. https://doi.org/10.35833/MPCE.2019.000062
47. Wu J, Chen X, Badakhshan S, Zhang J, Wang P (2022) Spectral graph clustering for intentional islanding operations in resilient hybrid energy systems. IEEE Trans Ind Inform 19(4):5956–5964. https://doi.org/10.1109/TII.2022.3199240
48. Ciapessoni E, Cirio D, Kjølle G, Massucco S, Pitto A, Sforna M (2016) Probabilistic risk-based security assessment of power systems considering incumbent threats and uncertainties. IEEE Trans Smart Grid 7(6):2890–2903
49. Amiri GG, Mahdavian A, Dana FM (2007) Attenuation relationships for Iran. J Earthquake Eng 11(4):469. https://doi.org/10.1080/13632460601034049
50. FEMA (2003) Multi-hazard loss estimation methodology: Earthquake model. Department of Homeland Security
51. Cornell CA, Krawinkler H (2000) Progress and challenges in seismic performance assessment. PEER Center News 3(2):1–3
52. Modarres M, Kaminskiy MP, Krivtsov V (2016) Reliability engineering and risk analysis: a practical guid. CRC Press
53. Li W (2013) Reliability assessment of electric power systems using Monte Carlo methods. Springer
54. Agency FEM, Resilience S (2021) Goals and Objectives for lifeline systems, FEMA P-1000. DC, USA, Washington
55. Hemmati M, Mohammadi-Ivatloo B, Abapour M, Anvari-Moghaddam A (2020) Optimal chance-constrained scheduling of reconfigurable microgrids considering islanding operation constraints. IEEE Syst J. https://doi.org/10.1109/JSYST.2020.2964637
56. Khaledi A, Saifoddin A (2023) Three-stage resilience-oriented active distribution systems operation after natural disasters. Energy 282:128360. https://doi.org/10.1016/j.energy.2023.128360
57. Du Y, Li F, Zheng T, Li J (2020) Fast cascading outage screening based on deep convolutional neural network and depth-first search. IEEE Trans Power Syst. https://doi.org/10.1109/TPWRS.2020.2969956
58. Zaini FA, Sulaima MF, Razak IAWA, Zulkafli NI, Mokhlis H (2023) A review on the applications of PSO-based algorithm in demand side management: challenges and opportunities. IEEE Access 11:53373–53400. https://doi.org/10.1109/ACCESS.2023.3278261
59. Del Valle Y, Venayagamoorthy GK, Mohagheghi S, Hernandez JC, Harley RG (2008) Particle swarm optimization: basic concepts, variants and applications in power systems. IEEE Trans Evol Comput 12(2):171–195. https://doi.org/10.1109/TEVC.2007.896686
60. Gonzalez-Longatt FM, Rueda JL (2014) PowerFactory applications for power system analysis. Springer
61. Karimiparidari S, Zaré M, Memarian H, Kijko A (2013) Iranian earthquakes, a uniform catalog with moment magnitudes. J Seismol 17(3):897–911. https://doi.org/10.1007/s10950-013-9360-9
62. Mirzaei N, Gao M-T, Chen Y-T, Wang J (1997) A uniform catalog of earthquakes for seismic hazard assessment in Iran. Acta Seismol Sin 10:713–726
63. Savier JS, Das D (2007) Impact of network reconfiguration on loss allocation of radial distribution systems. IEEE Trans Power Deliv 22(4):2473–2480. https://doi.org/10.1109/TPWRD.2007.905370
64. Awad AS, El-Fouly TH, Salama MM (2014) Optimal ESS allocation and load shedding for improving distribution system reliability. IEEE Trans Smart Grid 5(5):2339–2349. https://doi.org/10.1109/TSG.2014.2316197
65. Calcara L, Pietro AD, Giovinazzi S, Pollino M, Pompili M (2018) Towards the resilience assessment of electric distribution system to earthquakes and adverse meteorological conditions. In: 2018 AEIT international annual conference. IEEE, pp 1–6